Supplemental Data

Spatiotemporal Regulation of Ras Activity Provides Directional Sensing

Sheng Zhang, Pascale G. Charest, and Richard A. Firtel

SUPPLEMENTAL EXPERIMENTAL PROCEDURES

Materials, DNA constructs, and gene disruption

Materials and GST-RBD(Raf1), GFP-RBD(Raf1), GST-RBD(RalGDS), GFP-PH(CRAC), PTEN-GFP, and GFP-LimE-Δcoil were described previously [2, 4, 21, 28]. GST-RBD(Byr2) was generated as a GST fusion by cloning nucleotides 1-360 of the cDNA sequence of *S. pombe* Byr2 (provided by S. Subramani), corresponding to the RBD, into pGEX-KG [29]. DdNF1-myc was generated by adding the sequence of the myc epitope to the C-terminus of the full-length *nfaA* genomic DNA. The *nfaA* gene was disrupted by inserting a blasticidin resistant cassette into a *Bam*HI site created at nucleotide 1365 of the *nfaA* genomic DNA. Potential knockouts were screened by PCR and confirmed by Southern blot. The dictyBase (dictybase.org) was screened for putative RasGAPs using the RasGAP domain of human p120GAP or NF1 (Genbank ™ accession numbers P20936 and P21359, respectively). We performed sequence analyses using the Blast, Smart, and SCAN programs and did the alignments with ClustalW.

Cell culture and biochemical assays

All *Dictyostelium* cell lines were cultured in axenic HL5 medium at 22°C. We obtained all transformants through electroporation and maintained them in 40 μg /ml G418, 70 μg/ml hygromycin, or both as required. PKB kinase and Ras-GTP pull-down assays have been described previously [2, 13, 28, 30]. GST-RBD (Raf1) was used to pull down active FLAG-RasB, myc-RasD, and FLAG-RasG, whereas GST-RBD (Byr2) (RBD of the yeast protein Byr2) was used to pull down activated FLAG-RasC and GST-RBD (RalGDS) was used to pull

down activated Rap1. Quantification of Ras and PKB activities were determined by densitometry and expressed as the ratio of Ras-GTP over total Ras and ^{32}P-H2B over PKB relative to the maximal activity determined for wild-type. The F-actin-enriched, Triton X-100-insoluble cytoskeleton fraction was isolated and measured as described previously [31]. For the FACS assay, cells were harvested from dishes and labeled with FITC-phalloidin, as described previously [25], and then resuspended in 1 ml 50 μg/ml propidium iodide (PI) solution containing 100 μg/ml RNase and incubated 30 min at 37°C prior to FACS. We performed analytic flow cytometric measurements using a FACSAria flow cytometer with a 488 nm coherent sapphire solid-state laser (Becton Dickinson, San Jose, CA). We detected green fluorescence (FITC-phalloidin) and red fluorescence (PI-DNA) through a 515-545 nm bandpass filter and a 600-620 nm bandpass filter, respectively. Data analysis was performed using FlowJo software (Tree Star, Inc.).

Chemoattractant stimulation assays

Chemotactic assays were performed and analyzed using DIAS as described previously [4, 20, 25-27]. For assaying directional sensing in LatB-treated cells, we pre-treated cells with 5 μM LatB for 30 min. A micropipette containing chemoattractant was positioned in the dish and gradually moved towards the cell. Once GFP-RBD accumulated at the side of the membrane closed to the micropipette and formed a stable fluorescent crescent, the micropipette was rapidly repositioned to the opposite side of the cell. We measured the kinetics of GFP-RBD membrane translocation and dissociation at both sides of the cell as the relative fluorescence intensity of membrane-localized GFP-RBD determined as the intensity difference between the plasma membrane and the cytosol pool.

Imaging acquisition

DIC images of cells were taken at intervals of 6 sec for 30 min using a confocal microscope (DM IRE2; Leica) equipped with an ORCA-285 camera (Hamamatsu Photonics) and an HCX plan Apo 1.25-0.75 40X

objective lens (oil CS; Leica). Images were captured using the SimplePCI software (Compix Inc., Imaging Systems) and analyzed with the DIAS software [27]. Fluorescence images were obtained using the above-mentioned microscope with an HCX plan Apo NA 1.40 63X objective lens (oil CS; Leica) and ORCA-ER or dual view OI-11-EM-equipped EM-CCD cameras for simultaneous imaging (Hamamatsu Photonics). We analyzed the images using the Metamorph software (Molecular Devices). Quantification of membrane or cortical localization of GFP fusion proteins was performed as described previously [2]. TIRFM (total internal reflection fluorescence microscopy) images were taken using a Nikon TE300 microscope equipped with a Nikon Laser TIRF Unit Prototype and a Cascade II:512 EM-CCD camera (Photometrics), and captured with Image-Pro Plus software (Media Cybernetics).

Supplemental References

2. Sasaki, A.T., Chun, C., Takeda, K., and Firtel, R.A. (2004). Localized Ras signaling at the leading edge regulates PI3K, cell polarity, and directional cell movement. J Cell Biol *167*, 505-518.
4. Funamoto, S., Meili, R., Lee, S., Parry, L., and Firtel, R.A. (2002). Spatial and temporal regulation of 3-phosphoinositides by PI 3-kinase and PTEN mediates chemotaxis. Cell *109*, 611-623.
13. Meili, R., Ellsworth, C., Lee, S., Reddy, T.B., Ma, H., and Firtel, R.A. (1999). Chemoattractant-mediated transient activation and membrane localization of Akt/PKB is required for efficient chemotaxis to cAMP in Dictyostelium. Embo J *18*, 2092-2105.
20. Sasaki, A.T., Janetopoulos, C., Lee, S., Charest, P.G., Takeda, K., Sundheimer, L.W., Meili, R., Devreotes, P.N., and Firtel, R.A. (2007). G protein-independent Ras/PI3K/F-actin circuit regulates basic cell motility. J Cell Biol *178*, 185-191.
21. Iijima, M., and Devreotes, P. (2002). Tumor suppressor PTEN mediates sensing of chemoattractant gradients. Cell *109*, 599-610.
25. Chung, C.Y., and Firtel, R.A. (1999). PAKa, a putative PAK family member, is required for cytokinesis and the regulation of the cytoskeleton in Dictyostelium discoideum cells during chemotaxis. J Cell Biol *147*, 559-576.
26. Takeda, K., Sasaki, A.T., Ha, H., Seung, H.A., and Firtel, R.A. (2007). Role of PI3 kinases in chemotaxis in dictyostelium. J Biol Chem *282*, 11874-11884.
27. Wessels, D., Voss, E., Von Bergen, N., Burns, R., Stites, J., and Soll, D.R. (1998). A computer-assisted system for reconstructing and interpreting the dynamic three-dimensional relationships of the outer surface, nucleus and pseudopods of crawling cells. Cell Motil Cytoskeleton *41*, 225-246.
28. Kae, H., Lim, C.J., Spiegelman, G.B., and Weeks, G. (2004). Chemoattractant-induced Ras activation during Dictyostelium aggregation. EMBO Rep *5*, 602-606.
29. Guan, K.L., and Dixon, J.E. (1991). Eukaryotic proteins expressed in Escherichia coli: an improved thrombin cleavage and purification procedure of fusion proteins with glutathione S-transferase. Anal Biochem *192*, 262-267.
30. Jeon, T.J., Lee, D.-J., Merlot, S., Weeks, G., and Firtel, R.A. (2007). Rap1 controls cell adhesion and cell motility through the regulation of myosin II. J. Cell Biol. *176*, 1021-1033.

31. Steimle, P.A., Yumura, S., Cote, G.P., Medley, Q.G., Polyakov, M.V., Leppert, B., and Egelhoff, T.T. (2001). Recruitment of a myosin heavy chain kinase to actin-rich protrusions in Dictyostelium. Curr Biol *11*, 708-713.

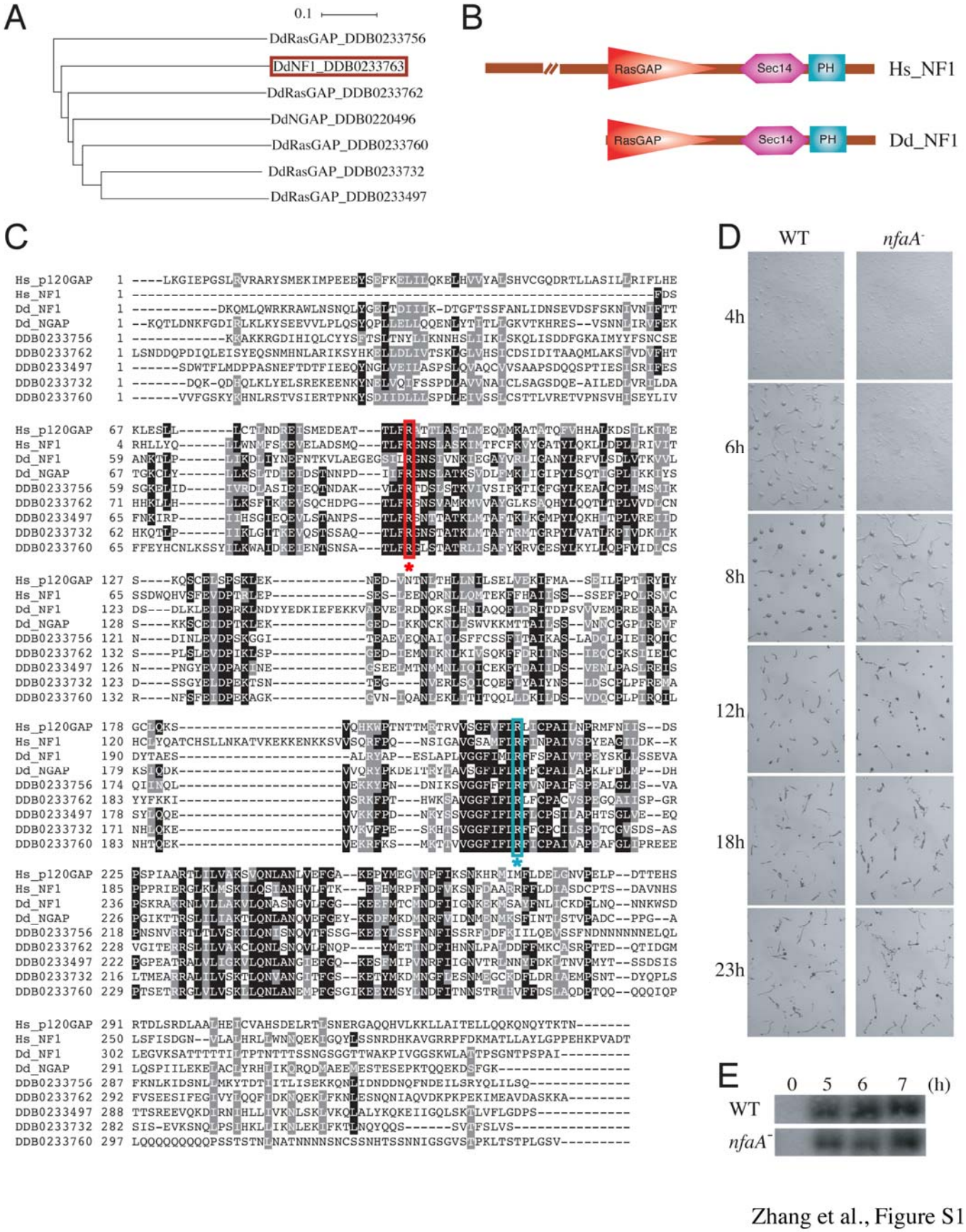

Zhang et al., Figure S1

Figure S1. DdNF1 Is a Putative Orthologue of the Human RasGAP NF1.

(A) Phylogenic tree of 7 putative *Dictyostelium* RasGAPs (DdRasGAP), including DdNGAP [32]. DdNF1 is highlighted. (B) Comparison of protein domains between human NF1 (Hs_NF1) and DdNF1. RasGAP, Sec14 (Sec14 homology), and PH (pleckstrin homology-like) domains are shown. (C) Sequence alignment of the catalytic RasGAP domain of human p120GAP and NF1, and the 7 putative *Dictyostelium* RasGAPs. * in red and blue indicates the invariant arginines corresponding to Arg^{789} and Arg^{903} in p120GAP, respectively. (D) Developmental phenotype of wild-type and *nfaA*$^{-}$ cells plated on non-nutrient agar. Starvation time is indicated. (E) Northern blot analysis of cAR1 (cAMP receptor 1) gene expression in wild-type and *nfaA*$^{-}$ cells pulsed with cAMP for the indicated time, suggesting that the expression of developmental genes is unaffected by the disruption of *nfaA*.

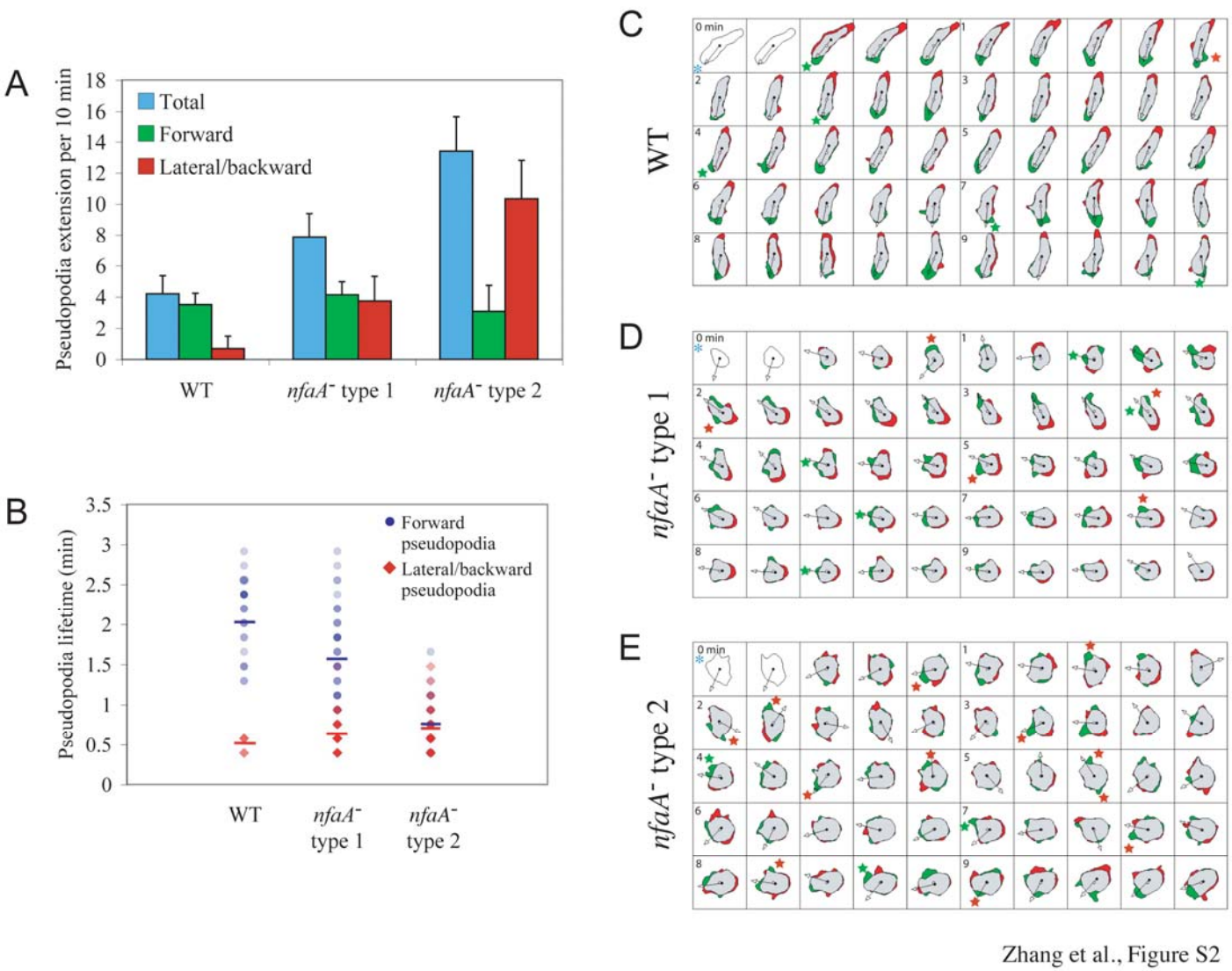

Figure S2. *nfaA*$^-$ Cells Produce Many Protrusions Laterally or Away from the Chemoattractant Source.

(A) Number of pseudopodia extended per cell migrating for 10 min in an exponential cAMP gradient. (B) Lifetime of extended pseudopodia. The shades reflect the relative amount of pseudopodia that displayed a similar lifetime, with the darker color corresponding to the highest number. (C-E) Shape difference analysis between each frame of recordings of representative wild-type or *nfaA*$^-$ (Type 1 and 2) cells migrating in an exponential cAMP gradient. Protrusions and retractions are illustrated in green and red, respectively, as determined by DIAS analysis [27]. Arrows from the cells' centroid indicate the direction of movement. *, direction of the gradient.

A

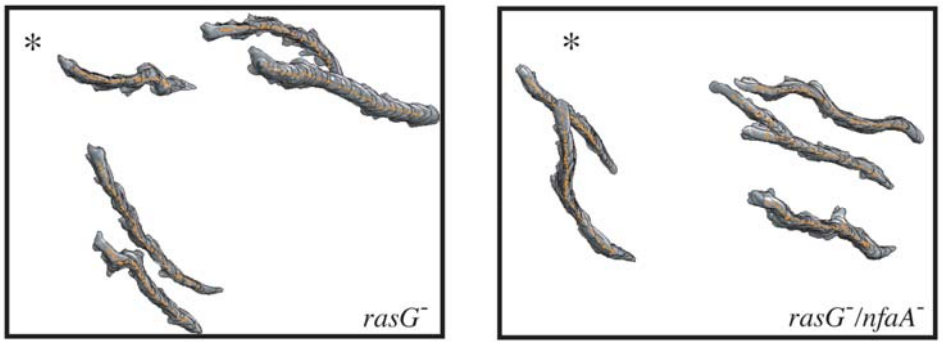

Strain	Chemotactic speed (μm/min)	Directionality	Direction change (deg.)	Roundness (%)
rasG⁻	7.52+/-1.48	0.84+/-0.05	24.3+/-8.0	52.8+/-11.0
rasG⁻/nfaA⁻	8.13+/-1.73	0.87+/-0.05	17.1+/-6.4	50.1+/-4.0

B

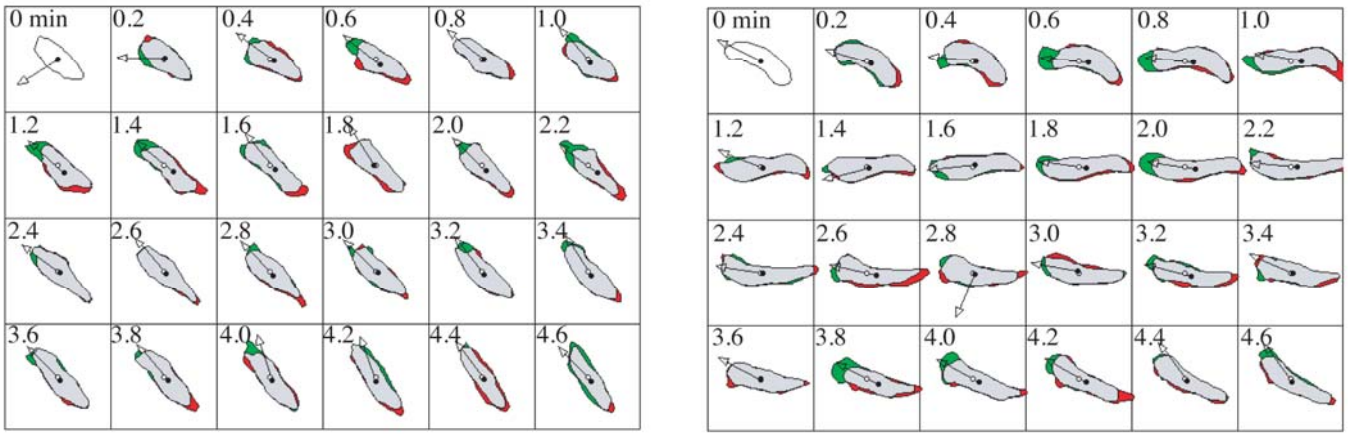

C

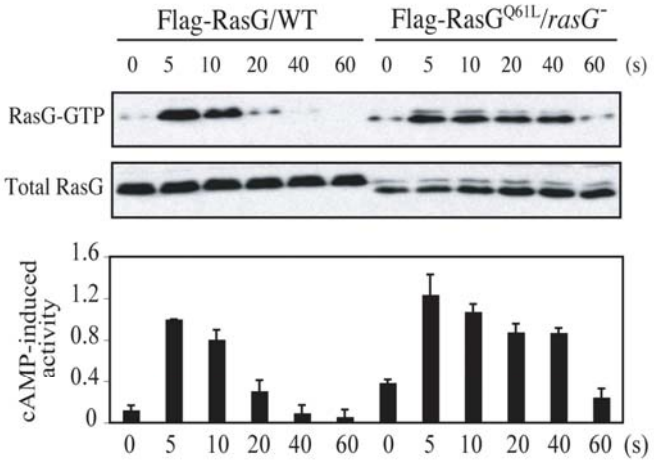

D

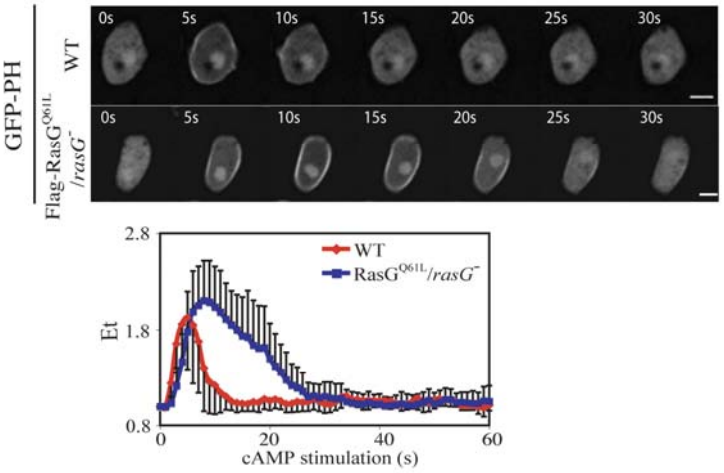

Zhang et al., Figure S3

Figure S3. The *nfaA*$^{-}$ Chemotaxis Phenotype Results From the Mis-Regulation of RasG.

(A) Traces of *rasG*$^{-}$ and *rasG*$^{-}$*nfaA*$^{-}$ cells chemotaxing in an exponential cAMP gradient. *, position of the micropipette. The table shows the results of the DIAS analysis [27] of 10 traces from at least 3 independent experiments. (B) Shape difference analysis between each frame of recordings of representative *rasG*$^{-}$ or *rasG*$^{-}$ *nfaA*$^{-}$ cells migrating in an exponential cAMP gradient. Protrusions and retractions are illustrated in green and red, respectively, as determined by DIAS analysis [27]. Arrows from the cells' centroid indicate the direction of movement. *, direction of the gradient. (C) Basal and cAMP-induced activity of FLAG-RasG and FLAG-RasG^{Q61L} expressed in *rasG*$^{-}$ cells assessed in a pull-down assay. The Ras proteins were detected by Western blot with and anti-FLAG (M2) antibody. Quantified data represent mean ± SD of 3 independent experiments. (D) Imaging of GFP-PH upon uniform cAMP stimulation in FLAG-RasG^{Q61L}/*rasG*$^{-}$ compared to wild-type cells. Bar = 5 μm. The relative fluorescence intensity of membrane-localized GFP-PH is shown on the right.

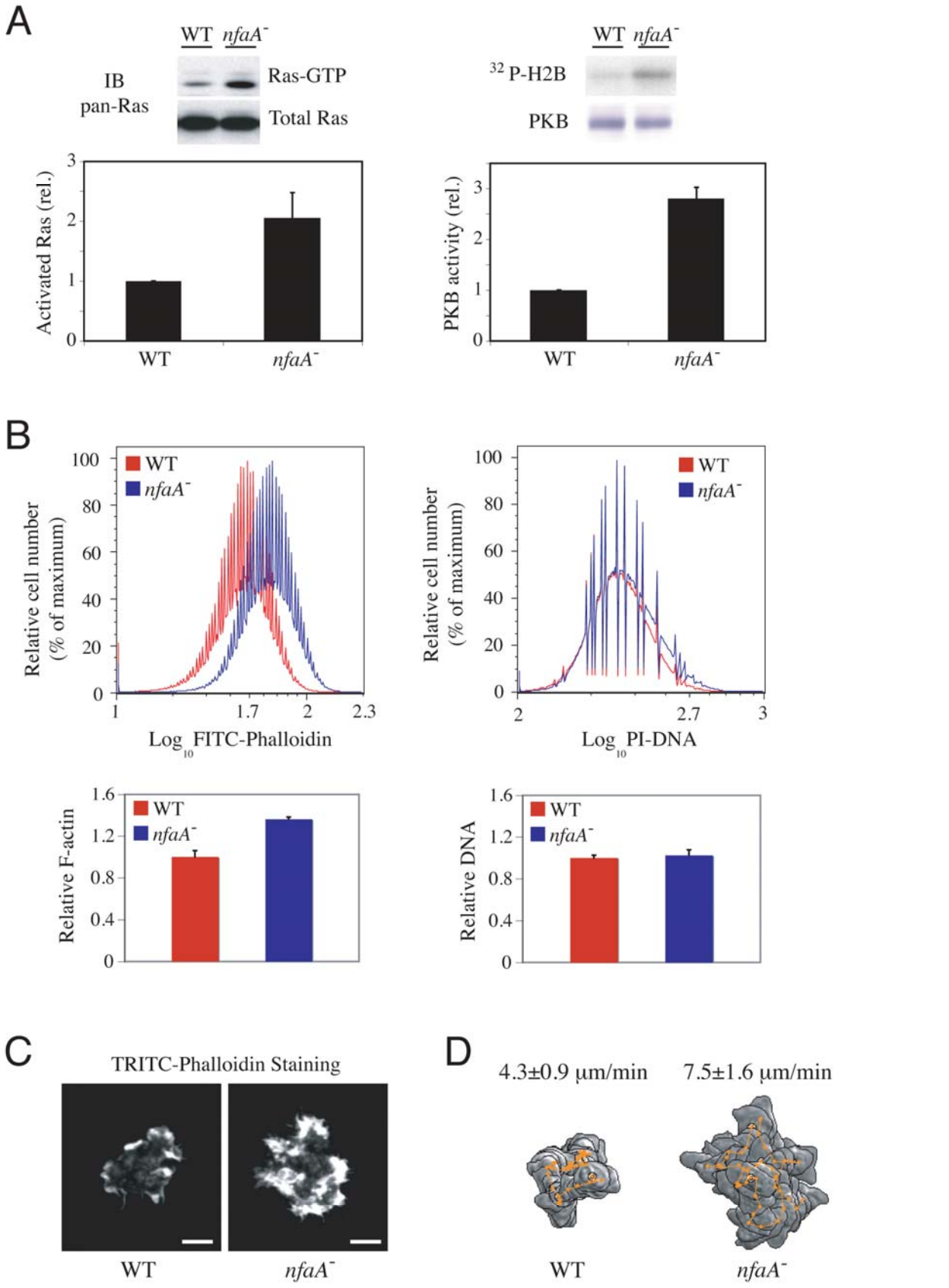

Zhang et al., Figure S4

Figure S4. RasGAP-Depleted Cells Exhibit Random Cell Motility Defects.

(A) Spontaneous Ras and PKB activities assessed and quantified as described in the legend to Figures 2 and 3. (B) F-actin levels determined by FACS. Green (FITC-phalloidin) and red (PI-DNA, an indicator of cell size) fluorescence histograms are shown. (C) Epifluorescent micrographs of TRITC-phalloidin-labelled cells. Bar = 5 μm. (D) Traces of representative randomly moving vegetative cells. The speed (movement of cell's centroid) was determined by analyzing 15 traces obtained from 3 independent experiments using DIAS software. Data represent mean ± SD of at least 3 independent experiments.

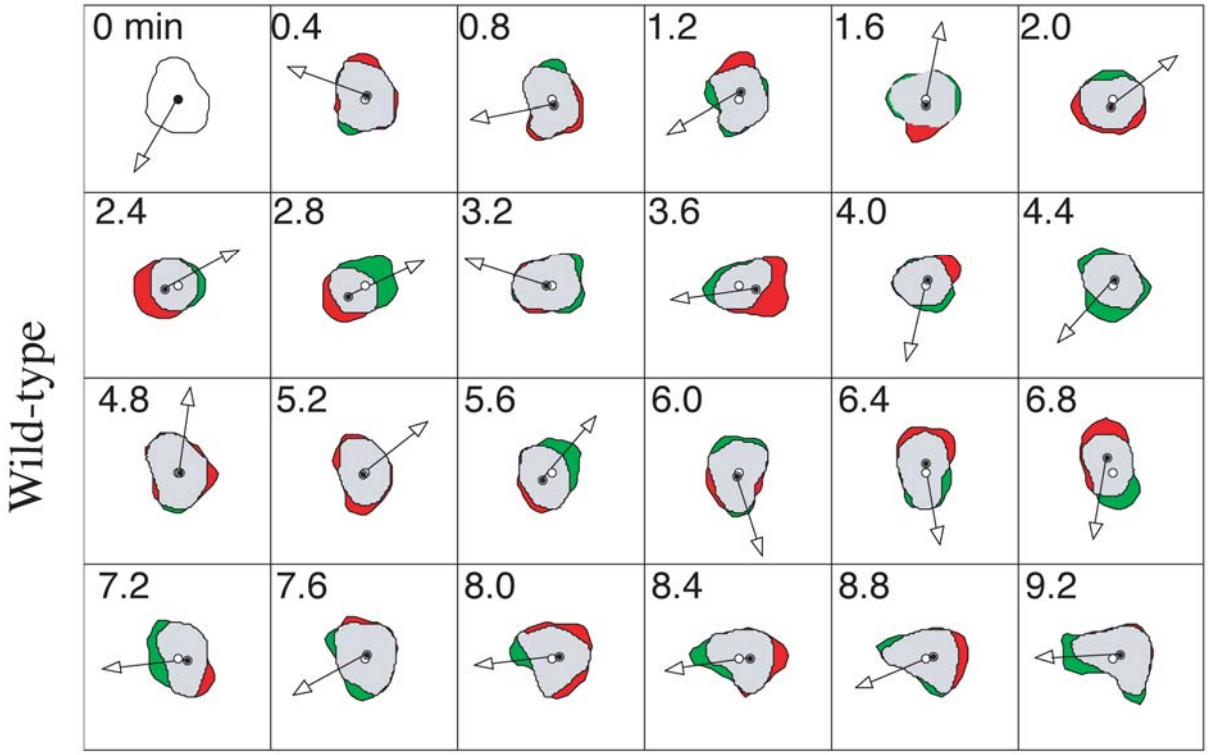

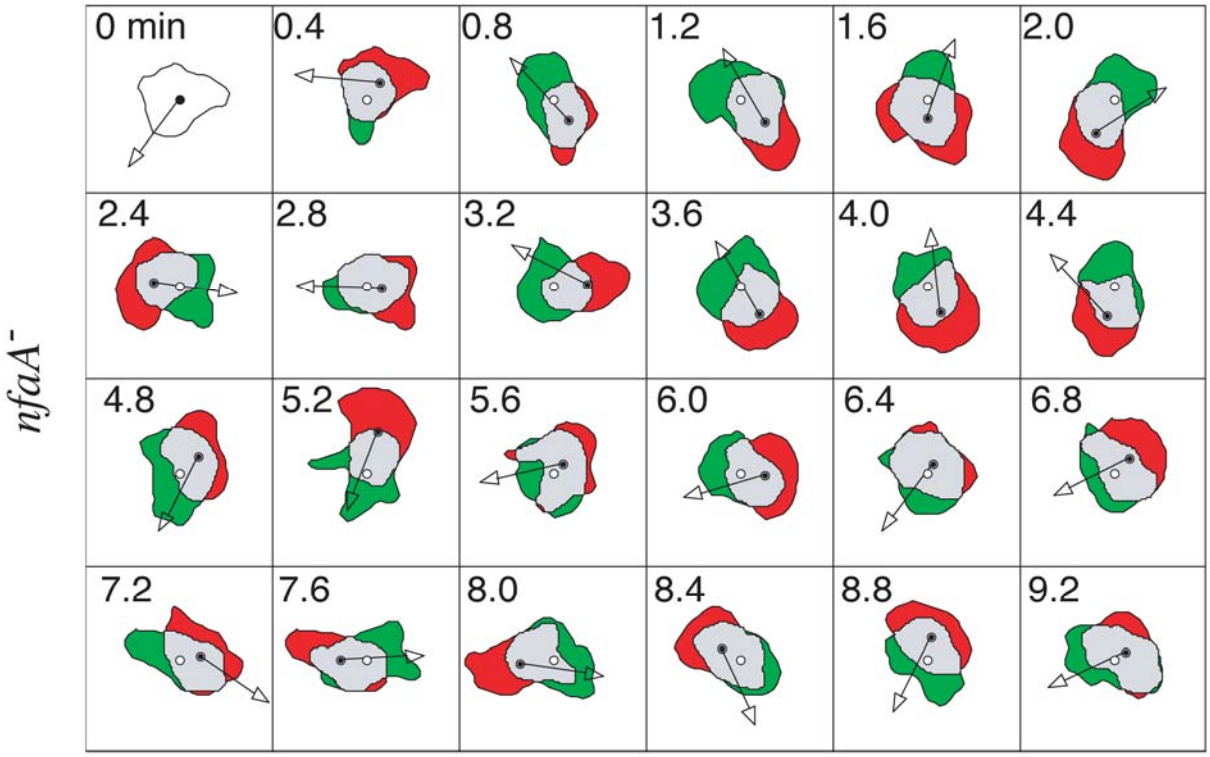

Zhang et al., Figure S5

Figure S5. Shape Difference Analysis of Randomly Moving Wild-Type and *nfaA*$^{-}$ Cells.

Images represent the shape difference analysis between each frame of recordings of representative vegetative cells undergoing random cell migration. Protrusions and retractions are illustrated in green and red, respectively, using DIAS analysis. Arrows from the cells' centroid indicate the direction of movement.

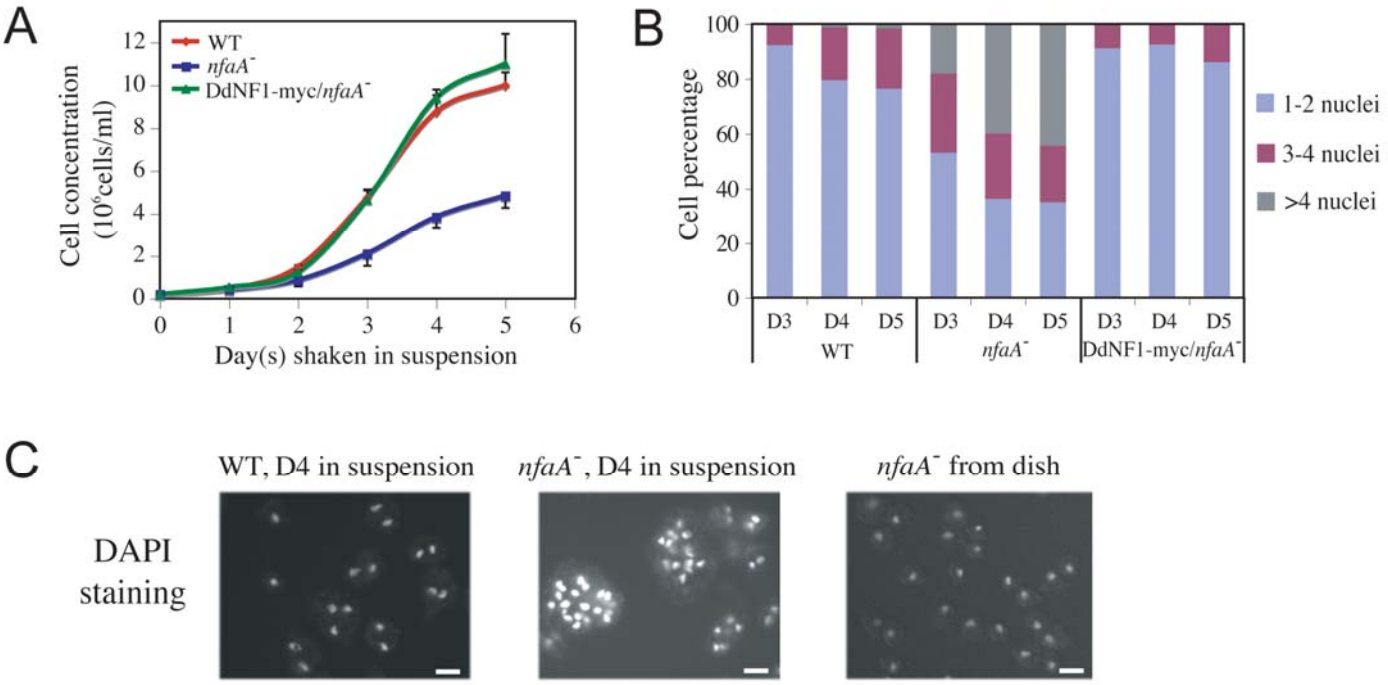

Figure S6. *nfaA*- Cells Display Cytokinesis Defects.

(A) Growth curves of suspension cell cultures of wild-type, *nfaA*-, and *nfaA*- cells expressing C-terminally myc-tagged DdNF1 (DdNF1-myc). Data represent mean ± SD of at least 3 independent experiments. (B) Number of nuclei per cell detected after 3, 4, and 5 days of growth in suspension, determined for at least 500 cells from 3 independent experiments. (C) Epifluorescent micrographs showing nuclei in cells grown in either suspension cultures for 4 days or on a Petri dish. Bar = 10 μm.

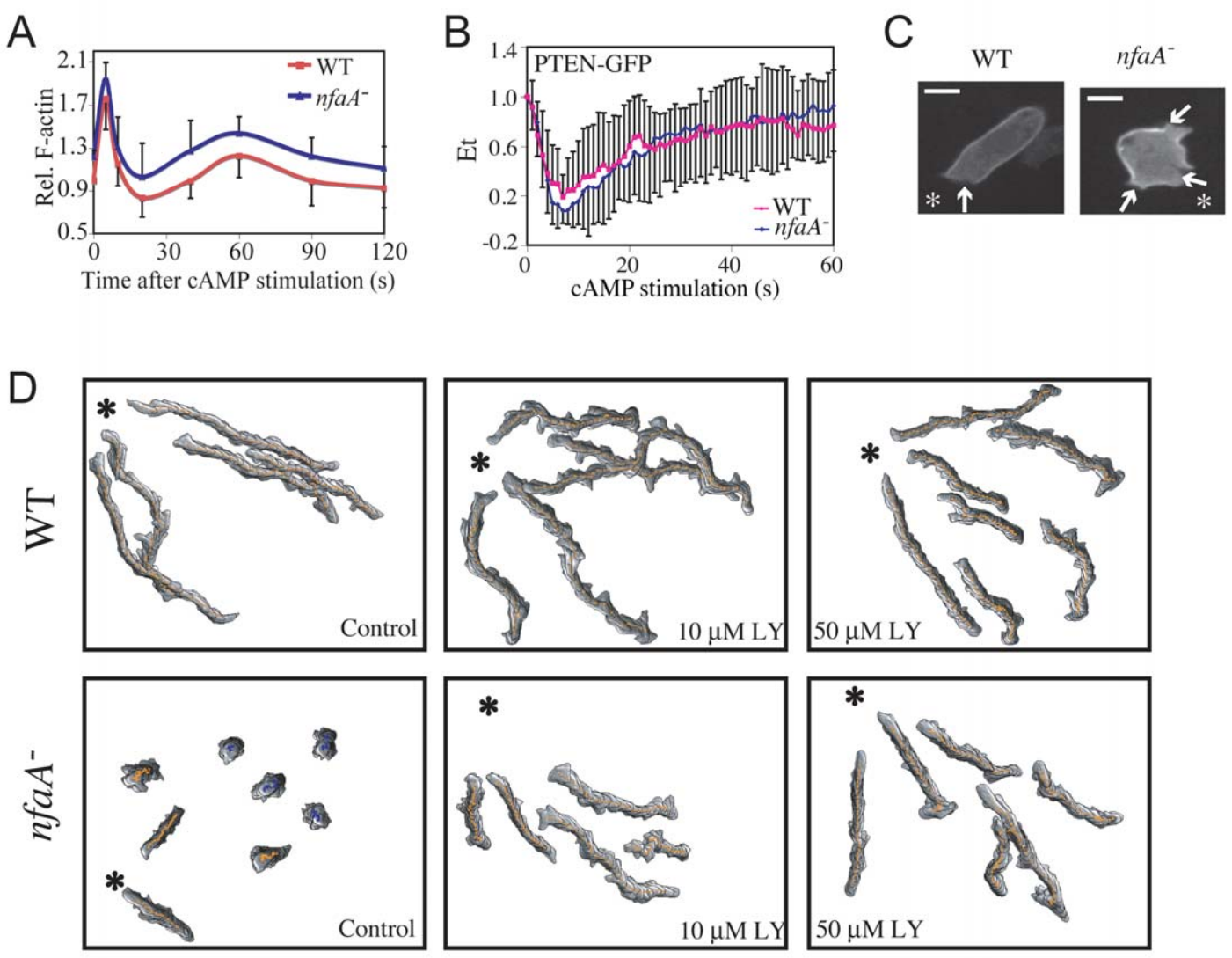

E

Strain	Chemotactic speed (μm/min)	Directionality	Direction change (deg.)	Roundness (%)
WT	14.05+/-2.70	0.89+/-0.05	12.1+/-3.3	50.6+/-5.2
nfaA⁻ type 1	4.08+/-1.45	0.56+/-0.29	42.0+/-19.9	72.5+/-6.7
nfaA⁻ type 2	2.74+/-0.98	0.20+/-0.09	53.1+/-4.5	80.8+/-2.8
10μM LY-treated WT	13.9+/-2.12	0.84+/-0.05	15.7+/-3.1	53.0+/-4.2
10μM LY-treated *nfaA*⁻	7.10+/-2.13	0.81+/-0.11	19.9+/-9.9	69.5+/-7.4
50μM LY-treated WT	8.71+/-1.95	0.85+/-0.08	15.6+/-4.6	64.3+/-5.0
50μM LY-treated *nfaA*⁻	7.68+/-1.64	0.77+/-0.11	26.2+/-6.7	60.3+/-5.0

Figure S7. The *nfaA*⁻ Chemotaxis Phenotype Results from the Mis-regulation of PI3K.

(A) cAMP-induced F-actin polymerization. Data represent mean ± SD of at least 3 independent experiments.

(B) Relative fluorescence intensity of membrane-localized PTEN-GFP upon uniform cAMP stimulation. Data

represent mean ± SD of at least 3 independent experiments. (C) Localization of PTEN-GFP in migrating cells. The images show that PTEN-GFP is absent from the leading edge and from the pseudopodia of chemotaxing wild-type and *nfaA*$^-$ cells, respectively. *, position of the micropipette. Arrows indicate membrane protrusions. Bar = 5 μm. (D) Traces of *nfaA*$^-$ cells chemotaxing in an exponential cAMP gradient emitted by a micropipette, treated either with the carrier alone (control) or with the indicated concentrations of LY for 30 min prior recording. *nfaA*$^-$ orange traces, type 1 cells; blue traces, type 2 cells. *, position of the micropipette. (E) DIAS analysis of at least 10 traces from at least 3 independent experiments of *nfaA*$^-$ cells, treated or not with LY, chemotaxing in an exponential chemoattractant gradient.

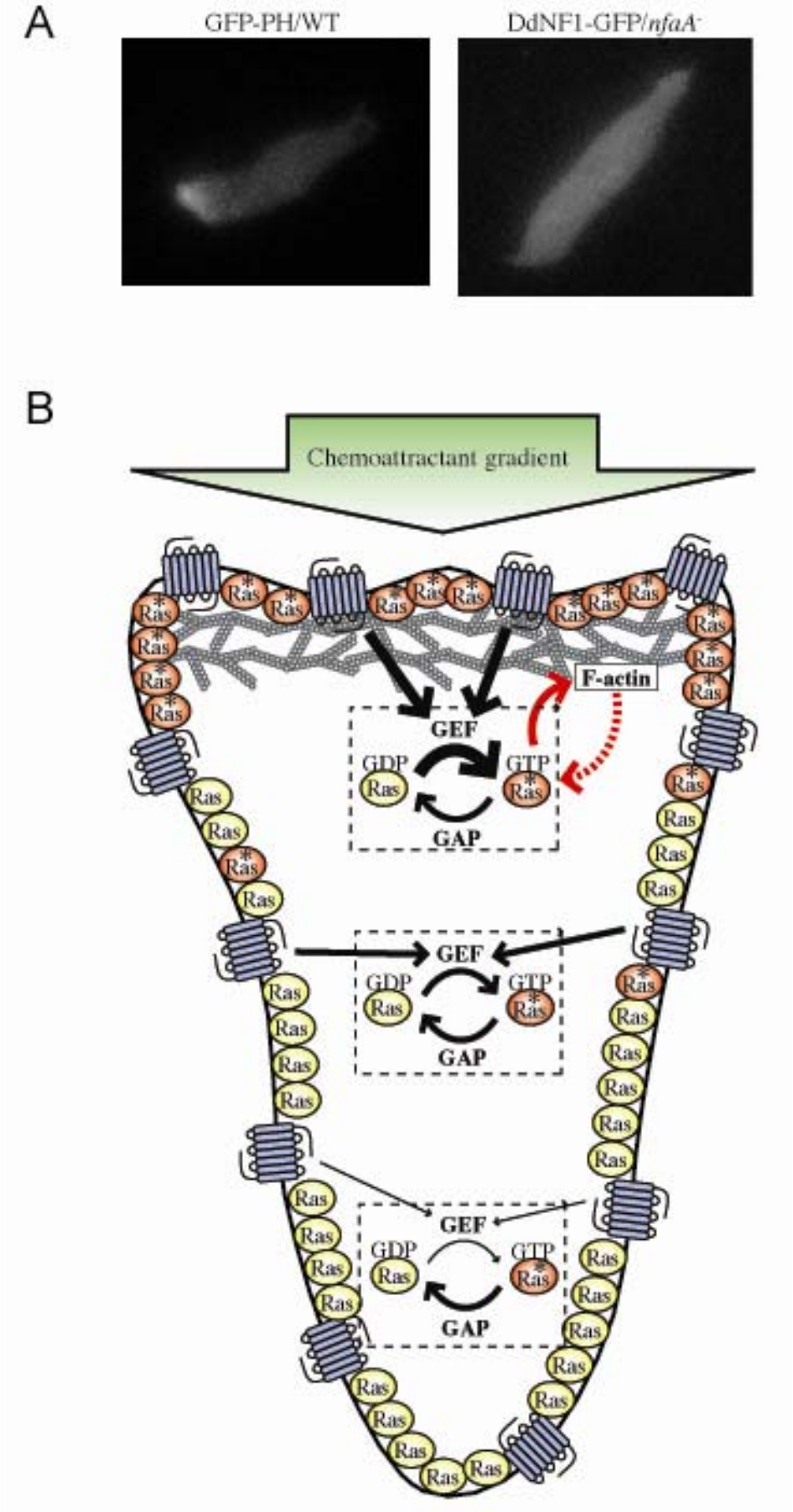
A
GFP-PH/WT
DdNF1-GFP/nfaA-
B
Chemoattractant gradient
F-actin
GEF
GDP
GTP
Ras
GAP

Figure S8. (A) TIRFM images of GFP-PH in wild-type cells and DdNF1-GFP in *nfaA*$^{-}$ cells chemotaxing under agar. The data show that membrane-localized DdNF1 is uniformly distributed in the chemotaxing cell unlike to GFP-PH, which is clearly enriched at the leading edge. (B) The GAP activity of RasGAPs, coupled to positive feedback loops from the cytoskeleton, creates a steep intracellular gradient of Ras activity in response to a chemoattractant gradient.